OBJECT DETECTION IN AIRBORNE LIDAR DATA FOR IMPROVED SOLAR RADIATION MODELING IN URBAN AREAS

Andreas Jochem[a,*], **Bernhard Höfle**[b], **Markus Hollaus**[b], **Martin Rutzinger**[c]

[a]University of Innsbruck, Department of Geography, 6020 Innsbruck, Austria
[b]Vienna University of Technology, Institute of Photogrammetry and Remote Sensing, 1040 Vienna, Austria
[c]International Institute for Geo-Information Science and Earth Observation, 7500 Enschede, The Netherlands

Commission III/2

KEY WORDS: Airborne LiDAR, 3D Point Cloud, Solar Potential, 3D Horizon, Segmentation, Vegetation

ABSTRACT:

In times of higher market prices of fossil fuels and to meet the increasingly environmental and economic threads of climate change renewable energy must play a major role for global energy supply. This paper focuses on a new method for fully automated solar potential assessment of roof planes from airborne LiDAR data and uses the full 3D information for both, roof plane detection and solar potential analysis. An image based candidate region detection algorithm reduces the data volume of the point cloud and identifies potential areas containing buildings with high completeness (97%). Three dimensional roof planes are extracted from the building candidate regions and their aspect and slope are calculated. The horizon of each roof plane is calculated within the 3D point cloud and thus shadowing effects of nearby objects such as vegetation, roofs, chimneys, dormers etc. are respected in a proper way. In contrast to other objects such as walls or buildings vegetation is characterized by transparent properties. Thus, in a further step vegetation is detected within the remaining non-roof points and transparent shadow values are introduced by calculating a local transparency measure averaged per tree segment. The following solar potential analysis is performed for regularly distributed roof points and results in both, (i) the annual sum of the direct and diffuse radiation for each roof plane and (ii) in a detailed information about the distribution of radiation within one roof. By calculating a clear sky index, cloud cover effects are considered using data from a nearby meteorological ground station.

1 INTRODUCTION

The increasing serious environmental and economic threats of climate change require new strategies concerning energy supply. Renewable energy must play a major role for global energy supply and has a positive effect on both, air quality and energy security and employment. Additionally, in times of higher market prices of fossil fuels, low-carbon alternatives will be competitive and there will be a rising demand for cost effective sustainable energy production.

In this contribution we present a new method for fully automated solar potential assessment of roof planes from airborne LiDAR data using the full 3D information of the point cloud for both, object detection and solar potential analysis. We aim at improving the methodology presented in Jochem et al. (2009) by introducing transparency for vegetation. By using the echo ratio of first-last pulse laser data as a measure of transparency we assume that vegetation is transparent if laser shots are reflected from within or below it. The algorithms are fully implemented in a geographic information system (GIS) and allow a combination of 2.5D raster data and 3D point cloud data. This paper describes the whole workflow, from object detection to solar radiation modeling in detail. The results will show the effect of considering transparent vegetation compared to the effect of considering vegetation solely as a solid object. The conclusion then states the major findings as well as future improvements, which can be introduced for solar radiation modeling.

2 RELATED WORK

This section presents previous studies concerning building detection, building reconstruction and solar potential analysis using LiDAR data.

In most cases building detection is performed on aggregated 2.5D grid data, which reduces the amount of the data of the 3D LiDAR data point cloud and makes processing less time consuming by using a simple data model. The complexity of the 3D space has not to be considered anymore but is irreversibly lost. By subtraction of a Digital Terrain Model (DTM) from a Digital Surface Model (DSM) a normalized Digital Surface Model (nDSM) is produced from which buildings are detected (e.g. Tovari and Vögtle, 2004; Abdullatif and James, 2002). Other authors identify buildings in the DSM using features such as local height jumps, curvature, height differences, local homogeneity of surface normals etc. (e.g. Matikainen et al., 2003; Rutzinger et al., 2006; Rottensteiner et al., 2005).
Buildings can also be detected in the 3D point cloud and the maximum achievable accuracy is maintained. Dorninger and Pfeifer (2008) assume that buildings are composed by a set of planar faces and developed a 3D segmentation algorithm, which detects planar faces in the point cloud. Building outlines are derived by projecting the detected points on the horizontal plane and applying a regularization algorithm. A combined raster and point cloud based analysis approach is utilized by Rutzinger et al. (2008). In a first step the advantages of the raster domain are used to extract building outlines, in order to reduce the data volume of the point cloud. The following 3D roof facet delineation is performed in the point cloud to provide the highest accuracy.

Building reconstruction can be performed using either (i) the model driven or (ii) the data driven approach. The model driven approach uses a predefined model library of basic building shapes and searches the most appropriate model among them (e.g. Maas and Vosselman, 1999; Tarsha-Kurdi et al., 2007). Thus, models are always topologically correct but complex shapes can not be reconstructed in a proper way because they are not included in the library. This approach is commonly applied for low point densi-

ties. The data driven approach allows to reconstruct buildings (regardless of its shape) without having a specified library (Tarsha-Kurdi et al., 2007) and is generally used for high point densities. A building is generated by identifying and intersecting neighboring roof segments, which are detected by segmentation algorithms (Dorninger and Pfeifer, 2008). Oude Elberink (2008) uses dense airborne LiDAR data (average point density of 25 points/m^2) to focus on problems related to the reconstruction of building parts.

There are many models performing solar potential analysis on basis of rasterized data and hardly any using the full 3D information of the point cloud. But with the arising of algorithms classifying and segmenting 3D LiDAR point cloud data automatically solar potential analysis can also be performed on a higher level of detail concerning the selection of suitable areas for the installation of solar panels. Kassner et al. (2008) mask roof contours within the LiDAR point cloud data by using building outlines. The remaining points are interpolated to a raster and analyzed according to slope, aspect and shaded areas.
Jochem et al. (2009) detect roof planes in the 3D point cloud and calculate aspect, slope and area of each roof facet. Solar potential analysis is performed for each plane using the full 3D information of the point cloud, without aggregating the 3D points to a 2.5D raster.

3 STUDY AREA AND DATASETS

The study area is located in the city of Feldkirch (Vorarlberg, Austria) and covers about 0.3 km^2 of urban settlement. The area is characterized by single houses and block buildings with mainly ridged roofs and vegetation of different crown shape and species. Roofs are overlapped by nearby vegetation in several cases. This can lead to challenges distinguishing between roofs and vegetation within the point cloud. The airborne LiDAR data were acquired under leaf-on conditions with a Leica ALS-50 scanner with a wavelength of 1064 nm, a pulse repetition frequency of 57 kHz, a maximum swath width of 75° and maximum scan rates of 75 Hz. The average point density within the study area is 17 points/m^2. Additionally, a Digital Terrain Model (DTM) and a Digital Surface Model (DSM) with 1m resolution each are available. The DTM is provided by the Federal State of Vorarlberg. The DSM is produced in GRASS GIS by aggregating the 3D point cloud to 2.5D raster cells, where the maximum elevation is chosen as cell value. A Digital Cadastral Map (DCM) is available as reference data set for evaluation of the building candidate region detection process.

4 METHODOLOGY

4.1 Workflow

Before performing solar potential analysis roof planes and vegetation have to be detected within the LiDAR data. An imaged based candidate region detection algorithm (Höfle et al., 2009) identifies coarse outlines of regions containing buildings. 3D roof planes are detected within these regions. In contrast to objects such as buildings vegetation is characterized by transparent properties. Hence, vegetation has to be detected and transparent shadow values are introduced. To respect shadows in a proper way the horizon of each detected roof point is calculated within the 3D point cloud. The workflow is shown in Figure 1. Detailed descriptions of each step are given below.

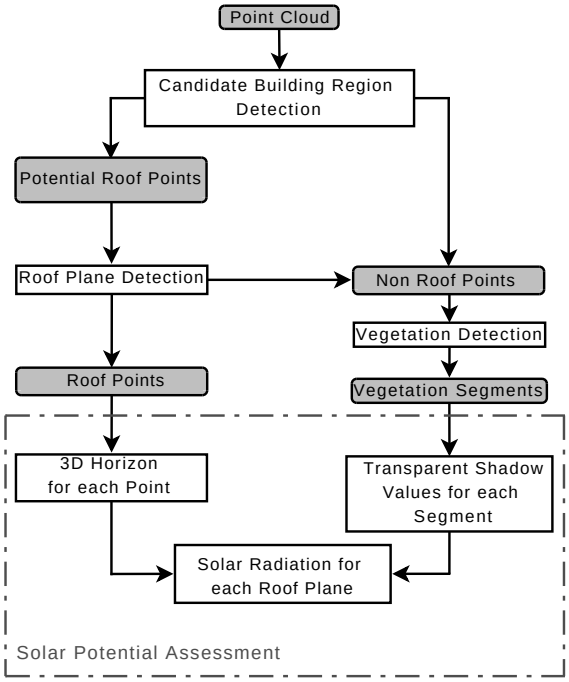

Figure 1: Workflow for object detection in 3D point cloud for solar potential assessment.

4.2 Candidate region detection

The candidate region detection algorithm was introduced by Höfle et al. (2009) and uses a GIS based raster analysis to find potential areas containing buildings. A slope-adaptive Echo Ratio (sER) value, which is a significant parameter for objects with low surface roughness (e.g. buildings) is derived for each laser point. The ER is defined as follows:

$$Echo\ Ratio\,[\%] = n_{3d} \,/\, n_{2d} \cdot 100 \qquad (1)$$

n_{3d}... number of points found in a fixed search distance measured in 3D
n_{2d}... number of points found in same distance measured in 2D

By dividing the initial 3D distance by the cosine of the local slope the sER is derived and a high value is guaranteed on steep solid surfaces. A sER raster layer is generated by aggregation of the derived values into regular cells whereas the mean sER value is taken per cell, in order to remove vegetation areas. Candidate regions are detected using a nDSM and the sER raster as input. By applying an object height and a sER threshold seed regions are identified, which are grown simultaneously to a defined maximum distance to include missing building parts such as dormers, chimneys or parts covered by vegetation. Finally, an object-based classification using a threshold on average laser point surface roughness is applied to remove non-building regions. Achieving full completeness (97%) of all buildings is favored over full correctness (59.6%), because the following roof plane detection is performed within the candidate regions. Figure 2 shows detected candidate regions compared to the DCM.

4.3 Roof plane detection

By selecting solely points within the candidate regions (Sect. 4.2) for roof plane detection the amount of point cloud data is drastically reduced (>80% reduction for the current test site). Roof planes are detected by decomposing the remaining point cloud

into homogeneous areas describing planar patches. To perform reliable solar potential analysis slope, aspect and area of each detected segment are calculated. In the following an overview of each step is given. Detailed descriptions can be found in Jochem et al. (2009).

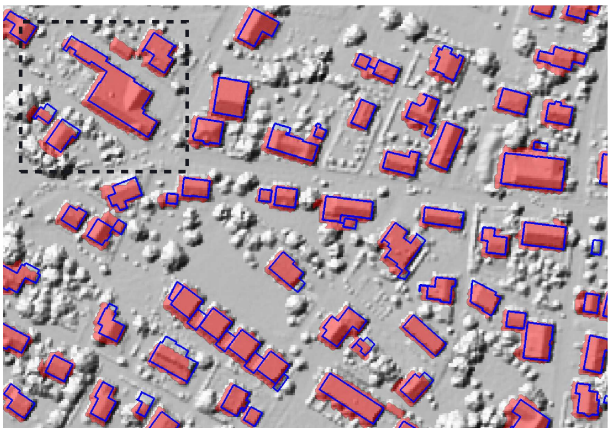

Figure 2: Detected candidate regions (red polygons) compared to the DCM (blue outlines). The black dashed rectangle indicates the location, which is examined in detail in the following sections.

4.3.1 Feature calculation: Assuming that roofs are composed of one or more planar patches the surface normal of each point is a good feature to subdivide the point cloud into homogeneous areas. By fitting an orthogonal regression plane to each point and its 3D *k* nearest neighbors the normal vector can be estimated. Points belonging to the same planar region must have similar normal vectors. Additionally, a surface roughness of each point is calculated to check its local planarity. It is defined as the standard deviation of the orthogonal fitting residuals.

4.3.2 Seed point selection and region growing: All points are sorted ascending by roughness. Only those points having a roughness value below a defined threshold are selected as potential seed points. The lower the roughness value the more likely the point lies on a planar face. The following region growing process is performed by checking candidate points (3D *k* nearest neighbors) by (i) similarity of normal vectors and (ii) 3D distance between current point and candidate point. A post processing step is introduced to detect points lying on roof ridges. Fixed distance (e.g. 1m) neighbors of each detected point on a roof plane (query point) are selected within the potential non-roof points. The orthogonal distance of each selected potential non-roof point is checked to the plane the query point belongs to. A point is assigned to a plane if it is within a defined distance threshold. If a point fulfills the distance criterion to one or more planes it is assigned to that plane to which the distance is the minimum. As one can see in Figure 3 also roof ridges are attached.

4.3.3 Calculation of slope, aspect and area The slope of each roof plane is defined as the angle between the horizontal plane (xy-plane) and the roof plane, which is fitted to the current segment. Aspect can be determined by projecting the normal vector of the segment on the xy-plane and calculating the angle (clockwise) from the y-axis. 2D Alphashapes (Edelsbrunner and Mücke, 1994) can be used to derive the outlines of an unorganized set of data points in 2D (Höfle et al., 2007; Da, 2006) and thus to calculate the area of a segment. The 3D points of a segment are projected orthogonal on its orthogonal regression plane followed by a projection on the xy-plane by maintaining the real size of the current segment.

4.4 Vegetation detection

Vegetation is detected within the non-roof points (i.e. points within and outside candidate regions that are not assigned to a roof plane after post processing) by using a segmentation presented by (Höfle et al., 2008). It is based on the assumptions that (i) vegetation can be distinguished from other objects by its convex shape, (ii) the normalized height of the vegetation exceed a defined threshold and (iii) a certain vertical distribution within vegetation occurs. The segmentation is performed on 2.5D raster and uses a nDSM and an ER raster (Sect. 4.2) as input. An edge based segmentation is processed by calculating the curvatures of the DSM and thresholding it to detect concave areas, which separate trees or groups of trees from each other. The degree of canopy structure detail is determined by the chosen window size (5x5) and the applied threshold on curvature. The final edge map, which represents the potential most exterior boundaries of a segment is intersected with those regions lying above the height threshold ($>$2 m) and echo ratio ($\geq$70%) threshold. A minimum number of points (100 points) per segment is applied to remove points that are recognized as vegetation but belong to part of a roof and have not been detected by the roof detection algorithm i.e. small dormers, roof edges, chimneys etc. In Figure 3 a 3D view of detected vegetation and detected roof planes is shown.

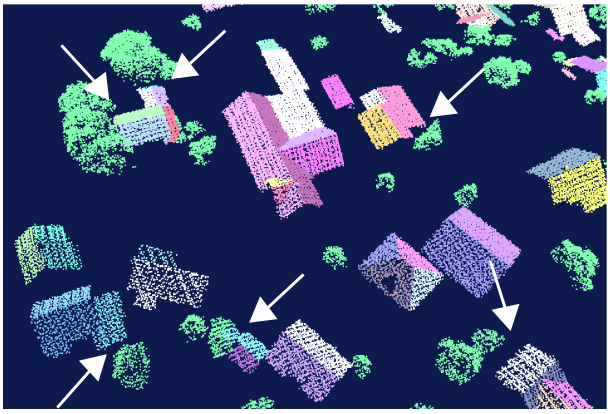

Figure 3: Point cloud view of detected roof planes together with detected vegetation (green). Arrows indicate roofs, which are possibly influenced by shadowing effects of nearby high vegetation.

5 SOLAR POTENTIAL ASSESSMENT

5.1 Theory

In this paper the global solar radiation of a point of interest is calculated by the sum of the direct and the diffuse radiation. The direct radiation is defined as the part of the radiation which reaches the surface directly without being reflected by the atmosphere. The diffuse radiation is reflected radiation reaching the surface. Formulas estimating both, the direct and the diffuse radiation are taken from Hofierka and Šúri (2002). The SOLPOS Code which was developed by the National Renewable Energy Laboratory (NREL, 2002) is used to calculate the position of the sun and its incidence angle on the surface of interest. By calculating a clear sky index (CSI), cloud cover effects are considered using data from a nearby meteorological ground station. The CSI is used to correct the modeled global solar radiation and differs from horizontal to inclined surfaces. On horizontal surfaces it is defined as the ratio of the global radiation under overcast conditions G_h and clear sky conditions G_{hc}. On inclined surfaces

the ratio of direct and diffuse radiation is different. Hence, these components have to be treated separately and the CSI has be computed for both, the direct and the diffuse radiation. Due to lack of meteorological data the CSI, which is computed for horizontal surfaces is also used to correct the values of inclined surfaces. It is estimated for every single day of the year. Once it is determined the global radiation of roof planes under overcast conditions can be estimated.

5.2 Uniform distribution of points

A uniform distribution of the recorded laser points can not be generally assumed. The distance between the points and the point density vary due to overlapping flight strips and changing airplane attitude. To avoid an over representation of a roof when calculating the arithmetic mean we propose a discretization of the derived roof planes. Thus, uniformly distributed points were placed in 3D space within the boundaries of each roof segment. In the following these points are called *uni-points*.

5.3 Shadowing effects

The major aim of this paper is to improve solar potential assessment of roof planes by respecting shadowing effects in a proper way. This includes (i) shadows of nearby object, (ii) shadows of the surrounding terrain and (iii) the introduction of transparent shadow values in order to take the transparent properties of vegetation into account. In the following each of these points is described in detail.

5.3.1 Shadowing effects of terrain: Shadowing effects of the terrain are not respected directly. They are included in the CSI. The global radiation under clear sky conditions on a horizontal surface (very close to the meteorological ground station) is computed by considering the shadows of a DTM. Values under overcast conditions are represented by 30-years measurements of the global radiation of a nearby meteorological ground station. This procedure is chosen, because on clear sky days the meteorological ground station is also affected by shadowing effects of the surrounding terrain. If one does not consider these shadows in the CSI, it will be underestimated. The CSI is calculated for every single day of the year.

5.3.2 Shadowing effects of nearby objects: Shadows of nearby objects are variable for each roof plane and are respected in a proper way by determining the horizon of each *uni-point* in the original 3D point cloud. The modeling of the horizon for one *uni-point* is illustrated in Figure 4. In a first step all points, which are found in a fixed search distance measured in 2D (e.g. 60 m) from the current *uni-point* (point of interest) are selected from the original point cloud. The distance and the difference in height to each of the selected points is checked in order to determine the angle δ, which is enclosed by the horizontal plane and the connection line between the current *uni-point* and the current selected point. The azimuth angle is defined as the angle (measured clockwise) between the current connection line and the y-axis. The azimuth angles are classified into classes of defined degree intervals (0.3). Furthermore, it is assumed that each point from the original point cloud is of a defined size (e.g. 0.3 m). Therefore, two *virtual points* (having the same height as the selected one) are placed in defined orthogonal distance (e.g. 0.15 m) to the connection line on each side of the current selected point, whereas the line connecting the virtual points runs through the current selected point. The angle δ, which is determined for the current selected point will be assigned to the azimuth classes affected by the line connecting the left and the right virtual point. If the value of delta of an azimuth class, which is currently affected is exceeded it will

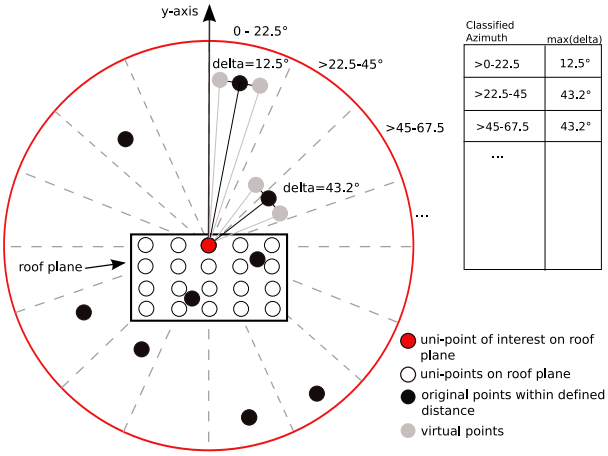

Figure 4: Schematic calculation of delta for one uni-point.

be overwritten. The default value for each azimuth class is zero. This procedure is repeated for each *uni-point*. Thus, one gets the minimum solar elevation angle (i.e. maximum value of δ) for each azimuth direction, which is required so that the current *uni-point* is not in the shadow. This procedure takes into account that points being closer to the current *uni-point* have a greater influence concerning shadowing effects (i.e. affect more azimuth classes) than those points being in the far distance. Points that have no neighbors in a defined search distance because they were reflected from e.g. birds, lanterns etc. are not considered to calculate δ. This avoids that single points cast a shadow on the *uni-point* like a high object. If there are powerlines within the area, eigenvalues could be used to extract linear features (Pfeifer and Briese, 2007) and exclude those points. Furthermore, a defined minimum distance (e.g. 0.3 m) from the current *uni-point* to a selected point is required. This avoids points, which are very close to the *uni-point* and differing in elevation due to noise casting a shadow.

5.3.3 Transparent shadow values: Transparent shadow values are introduced to take the transparent properties of vegetation in contrast to other objects such as buildings, walls etc. into account. We assume that vegetation is transparent if laser shots were reflected from within or below it. Thus, the ER (Equation 1) can be used to derive transparency, which is defined as follows:

$$Transparency\,[\%] = 100 - ER \qquad (2)$$

The mean transparency is calculated for each vegetation segment (Sect. 4.4) using the ER values of the respective laser points. A transparency value of zero is assigned to all non-vegetation points, which are considered as solid objects.
Transparency of each point is checked during the calculation of the horizon of each *uni-point* (Sect. 5.3.2). If a point casts a shadow its transparency value is stored as an additional feature. Hence, one gets the required information for each *uni-point* to perform reliable solar potential analysis. This includes the minimum solar elevation angle for any azimuth direction and its corresponding transparency value.

5.4 Solar potential analysis

Solar potential assessment is performed for each *uni-point* of a segment i.e. each point is treated separately. All *uni-points* of a segment are characterized by having equal inclination and aspect angles (i.e. the roof plane inclination and aspect). Thus, noise

occurring during measurement is suppressed and does not influence the solar potential analysis. Furthermore, the fact that solar panels are planar facets is also considered. The incoming global solar radiation is calculated for each day of the year from sunrise till sunset in one hour steps. Shadowing effects are checked by comparing the current solar elevation angle with the minimum required solar elevation angle (Sect. 5.3.2) for the current azimuth direction. If the current *uni-point* is within a shaded area the incoming direct radiation on that point is multiplied with the corresponding transparency value. The diffuse radiation remains unchanged. As a result one gets the annual global radiation on each *uni-point*. By multiplying the arithmetic mean of the global solar radiation per roof segment with its size the available solar energy per roof segment is calculated.

6 RESULTS AND DISCUSSION

A fundamental result of this paper is that the full 3D information of the point cloud can be used to model the global solar radiation of roof facets. A candidate building detection algorithm is applied to detect potential building areas, which serve to reduce the amount of data of the point cloud for further processing. A completeness of 97.0% and a correctness of 59.6% is achieved by using the DCM as reference layer. The low correctness value is due to several facts: (i) full completeness is favored over full correctness (i.e. the regions are overestimated), (ii) the DCM contains the building outlines represented by the walls, whereas LiDAR data contain the outlines represented by the roofs and (iii) dense vegetation having a high sER is also recognized as building area. Roof plane detection is performed in 3D within the candidate regions. The detection of vegetation in order to introduce transparent shadow values and to calculate the horizon in 3D are necessary steps to respect shadows in a proper way. Using a nDSM to calculate shadow masks would lead to deviations at roof overhangs, chimneys etc. due to rasterization of the point cloud. Figure 5 shows a result of the solar potential assessment. The incoming global solar radiation is calculated by taking transparency of vegetation into account. Parts that are covered by shadows of e.g. vegetation or/and building parts receive less solar energy than uncovered ones. Figure 6 shows the differences between the results of solar radiation modeling by considering and by not considering transparent shadow values. It is clearly visible

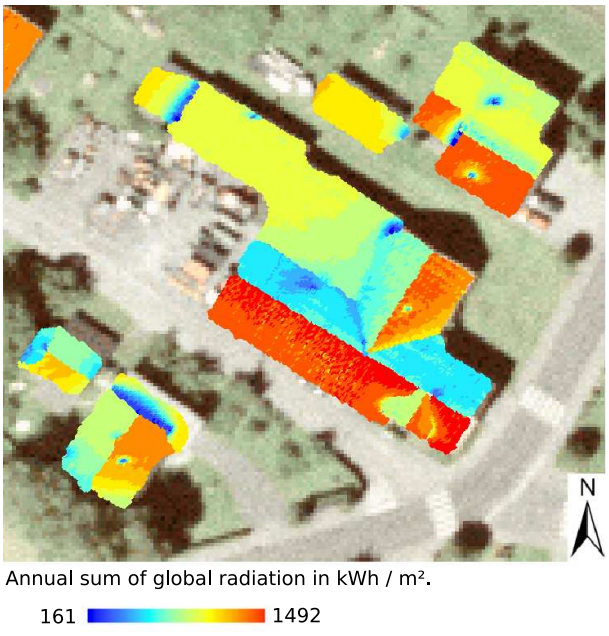

Figure 5: Annual sum of incoming global solar radiation on roof planes in kWh/m^2 by considering transparent properties of vegetation.

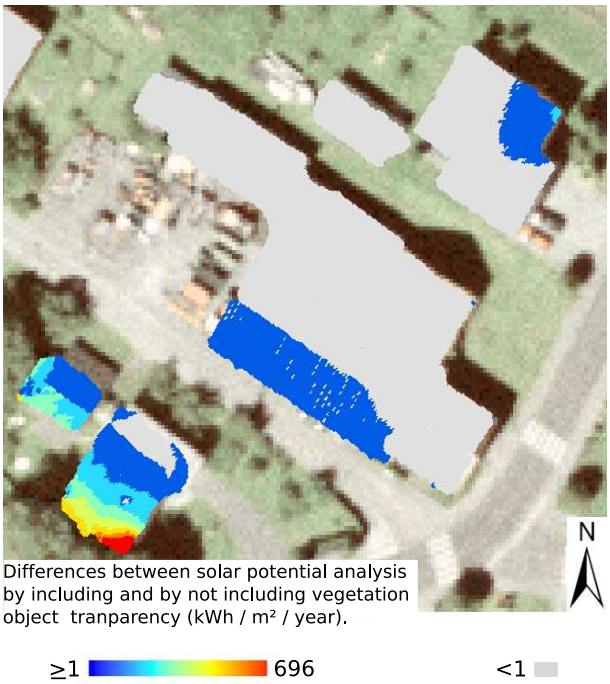

Figure 6: Differences in global solar radiation modeling between the results by respecting and by not respecting transparent properties of nearby vegetation. Gray colored areas are not influenced by shadows of vegetation.

that parts of a roof, which are strongly influenced by shadows of vegetation receive far more energy by including vegetation object transparency than by considering vegetation as solid objects. The increase in annual solar energy supply is around 696 kWh/m^2 for some roof parts (Figure 6 lower left roof). Hence, these roof parts are possibly suitable for the installation of solar panels and are not excluded a priori. Roof parts, which are only affected by shadows of building parts remain unchanged. The northern roof plane of the lower left roof in Figure 6 is mainly affected by shadows of the overlying roofs. Shadows of vegetation play a negligible role. Even if the height of the nearby vegetation is reduced this part will not gain more solar energy, whereas other roof parts would profit from it.

This paper is based on LiDAR data, which were acquired under leaf-on conditions. Hence, the computed transparency values are only adequate during leaf-on periods. The dependency of transparency of vegetation on time of the year is not considered yet. Improvements concerning transparency can still be made. Having LiDAR data from the same region under both, leaf-on and leaf-off conditions would lead to different transparencies of deciduous trees in winter and the values can be adjusted. A deciduous-coniferous tree classification (e.g. Liang et al., 2007) can also be performed, in order to model changing transparency of the corresponding vegetation. Deciduous trees would have increased transparency in winter, whereas the value of coniferous trees would remain constant. The ratio in transparency between leaf-on and leaf-off conditions for deciduous trees can be calculated by e.g. using a Terrestrial Laser Scanner (TLS) in order to estimate canopy gap fraction in winter and in summer (Danson et al., 2007).

The CSI, which is used to correct the modeled solar radiation values of both, horizontal and inclined surfaces is calculated on basis of a horizontal plane. By having more detailed data from a nearby meteorological ground station, the CSI can be determined for diffuse and direct radiation separately and will lead to better results on inclined surfaces.

7 CONCLUSION AND OUTLOOK

In this paper object detection is carried out to perform reliable solar potential analysis by using the full 3D information of the point cloud. Although reference data of incoming solar energy on selected roof planes is missing the presented approach shows promising results concerning the modeling of shadowing effects in the point cloud. The introduction of transparency values for vegetation is based on the assumption that vegetation has transparent properties if laser shots were reflected from within or below it. Thus, the Echo Ratio is used as a measure for transparency. By including vegetation object transparency the results of solar radiation modeling changed drastically in regions that are strongly influenced by vegetation and thus, roof parts that are covered by vegetation are not excluded a priori for the installation of solar panels. But improvements can still be made. Future work will concentrate on (i) integrating the described improvements (Sect. 6) in solar radiation modeling and on (ii) verifying the modeled values of global solar radiation with reference data from selected roof planes in order to check its reliability.

ACKNOWLEDGEMENTS

The authors would like to thank the Federal State of Vorarlberg for supplying the LiDAR data. This project was financed by the Climate and Energy Fund of the Austrian Federal Government and carried out in the scope of the program ”Energie der Zukunft”.

References

Abdullatif, A. and James, B., 2002. Heuristic filtering and 3d feature extraction from lidar data. In: IAPRS, Vol. XXXIV (3A), Graz, Austria.

Da, T., 2006. 2d alpha shapes. In: C. E. Board (ed.), CGAL-3.3 User and Reference Manual.

Danson, M.-F., Hetherington, D., Morsdorf, F., Koetz, B. and Allgöwer, B., 2007. Forest canopy gap fraction from terrestrial laser scanning. IEEE GEOSCIENCE AND REMOTE SENSING LETTERS 4(1), pp. 157 – 160.

Dorninger, P. and Pfeifer, N., 2008. A comprehensiv automated 3d approach for building extraction, reconstruction, and regularization from airborne laser scanning point clouds. Sensors 8, pp. 7323 – 7343.

Edelsbrunner, H. and Mücke, E., 1994. Three-dimensional alpha shapes. ACM Transaction on Graphics 13(1), pp. 43 – 72.

Hofierka, J. and Šúri, M., 2002. The solar radiation model for open source gis: implementation and applications. In: Proceedings of Open source GIS - GRASS users conference 2002, Trento, Italy.

Höfle, B., Geist, T., Rutzinger, M. and Pfeifer, N., 2007. Glacier surface segmentation using airborne laser scanning point cloud and intensity data. In: IAPRS, Vol. XXXVI (3/W52), Espoo, Finland, pp. 195 – 200.

Höfle, B., Hollaus, M., Lehner, H., Pfeifer, N. and Wagner, W., 2008. Area-based parameterization of forest structure using full-waveform airborne laser scanning data. In: R. Hill, J. Rosette and J. Surez (eds), Silvilaser 2008: 8th international conference on LiDAR applications in forest assessment and inventory, Edinburgh, Scotland, pp. 227 – 235.

Höfle, B., Mücke, W., Dutter, M., Rutzinger, M. and Dorninger, P., 2009. Detection of building regions using airborne lidar - a new combination of raster and point cloud based gis methods. In: GI-Forum 2009 - International Conference on Applied Geoinformatics, Salzburg. accepted.

Jochem, A., Höfle, B., Rutzinger, M. and Pfeifer, N., 2009. Automatic roof plane detection and analysis in airborne lidar point clouds for solar potential assessment. Sensors pp. 1 – 21. submitted.

Kassner, R., Koppe, W., Schüttenberg, T. and Bareth, G., 2008. Analysis of the solar potential of roofs by using official lidar data. In: IAPRS, Vol. XXXVII (B4), Beijing, China, pp. 399 – 403.

Liang, X., Hyyppä, J. and Matikainen, L., 2007. Deciduous-coniferous tree classification using difference between first and last pulse laser signatures. In: IAPRS, Vol. XXXVI (3/W52). on CD.

Maas, H.-G. and Vosselman, G., 1999. Two algorithms for extracting building models from raw laser altimetry data. ISPRS Journal of Photogrammetry & Remote Sensing 54, pp. 153 – 163.

Matikainen, L., Hyyppä, J. and Hyyppä, H., 2003. Automatic detection of buildings from laserscanner data for map updating. In: IAPRS, Vol. XXXIV (3/W13), pp. 218 – 224.

NREL, 2002. Nrel 2000 - solpos documentation. Technical report, National Renewable Energy Laboratory, Center for Renewable Energy Resources Renewable Resource Data Center.

Oude Elberink, S., 2008. Problems in automated building reconstruction based on dense airborne laser scanning data. In: IAPRS, Vol. XXXVII (3A), Bejing, China, pp. 93 – 98.

Pfeifer, N. and Briese, C., 2007. Geometrical aspects of airborne laser scanning and terrestrial laser scanning. In: IAPRS, Vol. XXXVI (3/W52), Espoo, Finland, pp. 311 – 319.

Rottensteiner, F., Trinder, J., Clode, S. and Kubik, K., 2005. Automated delineation of roof planes from lidar data. In: IAPRS, Vol. XXXVI (3W/19), Enschede, The Netherlands, pp. 221 – 226.

Rutzinger, M., Höfle, B. and Pfeifer, N., 2008. Object detection in airborne laser scanning data - an integrative approach on object-based image and point cloud analysis. In: T. Blaschke, S. Lang and G. Hay (eds), Object-Based Image Analysis - Spatial concepts for knowledge-driven remote sensing applications, Springer, pp. 645 – 662.

Rutzinger, M., Höfle, B., Pfeifer, N., Geist, T. and Stötter, J., 2006. Object-based analysis of airborne laser scanning data for natural hazard purposes using open source components. In: IAPRS, Vol. XXXVI (4/C42), Salzburg, Austria. on CD.

Tarsha-Kurdi, F., Landes, T., Grussenmeyer, P. and Koehl, M., 2007. Model-driven and data-driven approaches using lidar data: analysis and comparison. In: IAPRS, Vol. XXXVI (3/W49A), Munich, Germany, pp. 87 – 92.

Tovari, D. and Vögtle, T., 2004. Object classification in laser-scanning data. In: IAPRS, Vol. XXXVI (8/W2), pp. 45 – 49.